# THE "MICROMORPH" CELL: A NEW WAY TO HIGH-EFFICIENCY-LOW-TEMPERATURE CRYSTALLINE SILICON THIN-FILM CELL MANUFACTURING?

H. Keppner, P. Torres, J. Meier, R. Platz, D. Fischer, U. Kroll, S. Dubail, J. A. Anna Selvan, N. Pellaton Vaucher, Y. Ziegler, R. Tscharner, Ch. Hof, N. Beck, M. Goetz, P. Pernet, M. Goerlitzer, N. Wyrsch, J. Veuille, J. Cuperus, A. Shah, J. Pohl*

Institut de Microtechnique, A.-L. Breguet 2, Université de Neuchâtel, CH-2000 Neuchâtel, Switzerland

*University of Konstanz, D-78434 Konstanz, Germany

ABSTRACT

In the past, microcrystalline silicon (μc-Si:H) has been successfully used as active semiconductor in entirely μc-Si:H p-i-n solar cells and a new type of tandem solar cell, called the "micromorph" cell, was introduced [1]. Micromorph cells consist of an amorphous silicon top cell and a microcrystalline bottom cell. In the paper a micromorph cell with a stable efficiency of 10.7 % (confirmed by ISE Freiburg) is reported.

Among sofar existing crystalline silicon-based solar cell manufacturing techniques, the application of microcrystalline silicon is a new promising way towards implementing thin-film silicon solar cells with a low temperature deposition. Microcrystalline silicon can, indeed, be deposited at temperatures as low as 220°C; hence, the way is here open to use cheap substrates as, e.g. plastic or glass. In the present paper, the development of single and tandem cells containing microcrystalline silicon is reviewed. As stated in previous publications, microcrystalline silicon technique has at present a severe drawback that has yet to be overcome: Its deposition rate for solar-grade material is about 2Å/s; in a more recent case 4.3 Å/s [2] could be obtained. In the present paper, using suitable mixtures of silane, hydrogen and argon, deposition rates of 9.4 Å/s are presented. Thereby the dominating plasma mechanism and the basic properties of resulting layers are described in detail. A first entirely microcrystalline cell deposited at 8.7 Å/s has an efficiency of 3.15%.

## 1. INTRODUCTION.

Microcrystalline Silicon (μc-Si:H) is generally obtained by using a strongly hydrogen-diluted silane discharge [3]. Apart from some isolated approaches [4, 5] presented in the past, μc-Si:H was never seriously taken into account as being able to play a role as active semiconductor in a solar cell; this was basically due to its generally high density of gap-states. On the other hand, microcrystalline silicon has since some time already been successful in providing highly doped p and n contacts, as needed for such devices as solar cells and thin film transistors (TFT). It should be emphasised that the Very High Frequency Glow-Discharge (VHF-GD) deposition technique can be considered to play an important role in obtaining "solar grade" μc-Si:H material [1, 6-10]

The deposition of "mid gap" material is not straightforward; as-deposited intrinsic μc-Si:H turns out to be slightly n-type. According to Veprek [11] this is basically due to oxygen impurities. Two techniques have in the past been tried out to overcome this problem:

1. The compensation technique: Adding small traces of diborane to the feedgas compensate the n-type behaviour [6].
2. The purifying technique: a gas purifier (oxygen getter) is installed close to the reactor in order to remove oxygen-containing impurities in the feedgas [12]. It can be concluded at the present

state, that the purifying technique has the capacity to completely replace the compensation technique.

## 2. SOLAR CELLS BASED ON MICROCRYSTALLINE SILICON: REVIEW OF PAST WORK

Striking features of the entirely microcrystalline solar cells deposited by VHF-GD using either the compensation method or the purifier method, are the following:

1. complete stability of the efficiency under intense long term light soaking; a property that sofar could never be achieved using amorphous silicon as base material (see Fig. 3 taken from Meier et al. [1]).
2. strongly enhanced extension of the spectral response towards infrared wavelengths, as compared to amorphous silicon (see Fig. 2, taken from Meier et al. [1]).

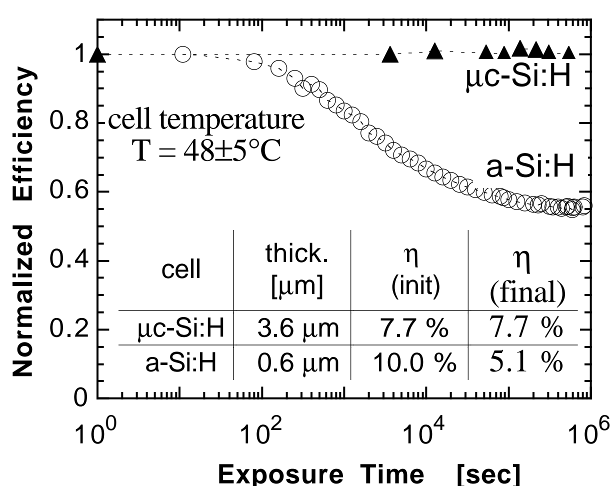


Fig. 1 Light-soaking of an amorphous and of a µc-Si:H cell under 6 and 10 suns respectively (According to Meier et al. [9]).

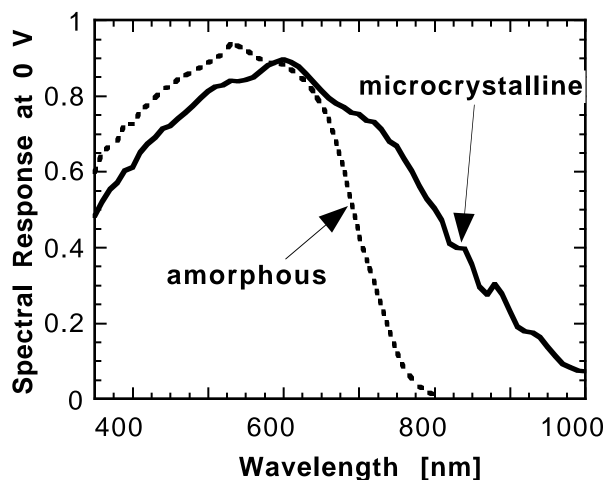


Fig. 2 Comparison of the spectral response of an a-Si:H cell and of an entirely microcrystalline cell (Meier et al. [1]).

The combination of an entirely microcrystalline solar cell used as bottom-cell with a "classical" amorphous silicon solar cell forms a "true" tandem cell; this combination is called by the authors a "micromorph" cell. Thereby, the top cell is rendered more stable using a relatively thin intrinsic amorphous layer deposited under strong hydrogen dilution. As shown in previous publications [7], the top cell alone gives rise to the full light-induced degradation of the total micromorph tandem cell. Table 1 gives an overview of the stable efficiencies sofar obtained for entirely µc-Si:H cells and micromorph tandem cells.

| cell type | η [%] | Isc | Voc | FF | area [cm2] | remark |
|---|---|---|---|---|---|---|
| µc-p-i-n | 7.7 | 25.3 | 0.448 | 67.9 | 0.33 | 10 suns, 48±5°C, 400 h |
| Micromorph | 10.7* | 11.0 | 1.359 | 63.0 | 0.33 | 1000 h Am 1.5; 50°C |

* Confirmed by the ISE Freiburg (D).

Tab. 1 Solar cell parameters of stable entirely µc-Si:H cells and of micromorph cells.

<u>Limits and potential for further improvements.</u>

From Tab. 1. one can conclude that the top cell produces about two thirds of the total output of the tandem cell [10]; this is based on the strong difference in Voc between top and bottom cell. From this fact, one has to deduce that the stability of the top cell remains a key feature, as long as

the open circuit voltage of the bottom cell remains limited. This also means that a further increase of the $V_{OC}$ of the bottom cell alone contains the highest potential for a further improvement of the stable efficiency of the micromorph cell. The strongest limitation in the future industrial potential of all types of thin-film crystalline silicon solar cells is, at present, the too long manufacturing times (recrystallization and/or deposition rates). For the deposition of μc-Si:H, the VHF-GD process in itself brings sofar at least some improvement, as reported by Finger et al. [13] Attempts at obtaining yet higher deposition rates are described by Torres et al. [2]. In this paper we present an alternative approach using argon plus hydrogen dilution of silane. Argon dilution and mixtures of Ar, $H_2$ and silane have often been reported in literature for a-Si:H deposition with the attempt to obtain more stable material [14]. As a beneficial effect Kroll et al. [15] report on significant silane savings using argon dilution. In another work, an increase of the deposition rate of a-Si:H due to Ar-dilution is reported by Hautala et al. [16]. For μc-Si:H, DC plasma gun experiments for high-rate deposition of μc-Si:H are reported by Imajyo [17]; in the latter case, a mixture of Ar, $H_2$ and $SiH_4$ was used. In other publications an enhanced dissociation of $SiH_4$ is reported due to molecular quenching via metastables [15, 18, 19]. In the latter case, a pure Ar / $SiH_4$ system was studied.

## 3. EXPERIMENTAL: PROCEDURES USED FOR ARGON /HYDROGEN DILUTION

All the experiments presented here were undertaken using the VHF-GD technique at 70 MHz in a parallel plate reactor. Three series were deposited; Tab. 2. shows the strategy used.
For the M-series (**M**ixing-series), the mixture of the diluting gases Ar and $H_2$ was varied at constant silane flow. (6 sccm). The sum of flows of the diluting gases (Ar + $H_2$) was 150 sccm.
For the D-series (**D**ilution-series), the mixture of the two diluting gases was kept constant, at 90 sccm $H_2$ and 60 sccm Ar, whereas the silane flow was varied.
For the P-series the **P**ower of the plasma was varied for a fixed silane flow of 8.4 sccm in 90 sccm hydrogen and 60 sccm Argon.

| Serie | $\Phi(SiH_4)$ [sccm] | $\Phi(H_2)$ [sccm] | $\Phi(Ar)$ [sccm] | Power [W] | Pressure [mbar] |
|---|---|---|---|---|---|
| **M** | 6 | **140 - 0** | **10 - 150** | 30 | 0.8 mbar |
| **D** | **6-12** | 90 | 60 | 40 | 0.9 mbar |
| **P** | 8.4 | 90 | 60 | **10 - 70** | 0.9 mbar |

Tab. 2. Strategy of $H_2$ / Ar dilution experiments for deposition of μc-Si:H.

Within the study of these series M, D, and P we will now lay the emphasis on plasma properties, deposition rate, structural properties of the μc-Si:H films (X-Ray measurements), infrared measurements, and sub-bandgap absorption (PDS).
In order to correlate the properties of the layers of series M, D and P with the corresponding properties of the plasma, optical emission spectroscopy was carried out. For this purpose, a monochromator with a detector was mounted at the VHF-reactor. Before every deposition, a new glass plate had to be inserted into the reactor in order to protect the window from being coated. The substrate and the powered electrode were heated up to 220°C. For this study, no gas purifier was applied.

## 4. RESULTS AND DISCUSSION

<u>Results on the deposition rate.</u>
In several publications a link between the intensity of the SiH* 412 nm emission line and the deposition rate of a-Si:H was shown (Perrin et al. [20]). Hamasaki et al. [21] reported on a criterion for the deposition of microcrystalline silicon if the relationship of the emission

intensities H(656nm)/Si(412nm) exceeds unity. As in our present study three gases ($SiH_4/H_2/Ar$) are involved, a criterion for the growth rate of µc-Si:H from the emission spectrum of these gases was looked for. Fig. 3 shows a typical OES (optical emission spectrum) of a $SiH_4$ / $H_2$ / Ar plasma. The lines of interest are therein particularly mentioned:

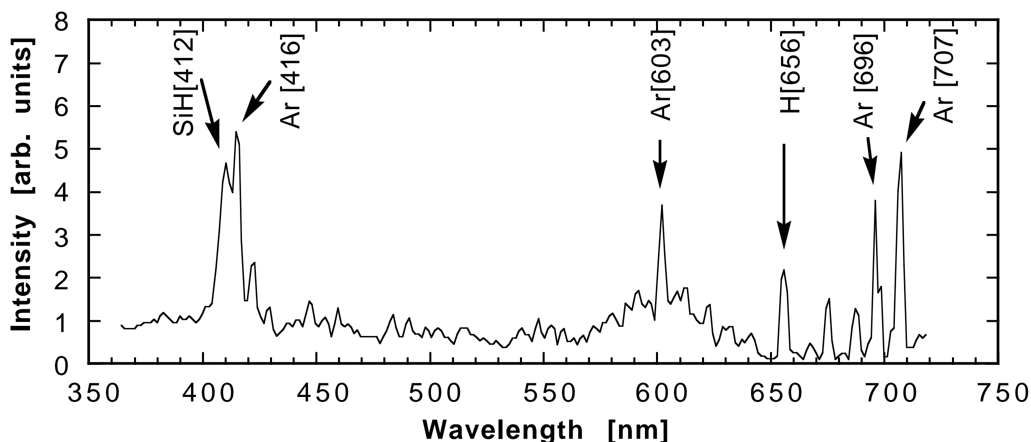


Fig. 3: Typical OES of a $SiH_4$ / $H_2$ / Ar plasma with the lines of interest for this study.

Result of M-series.

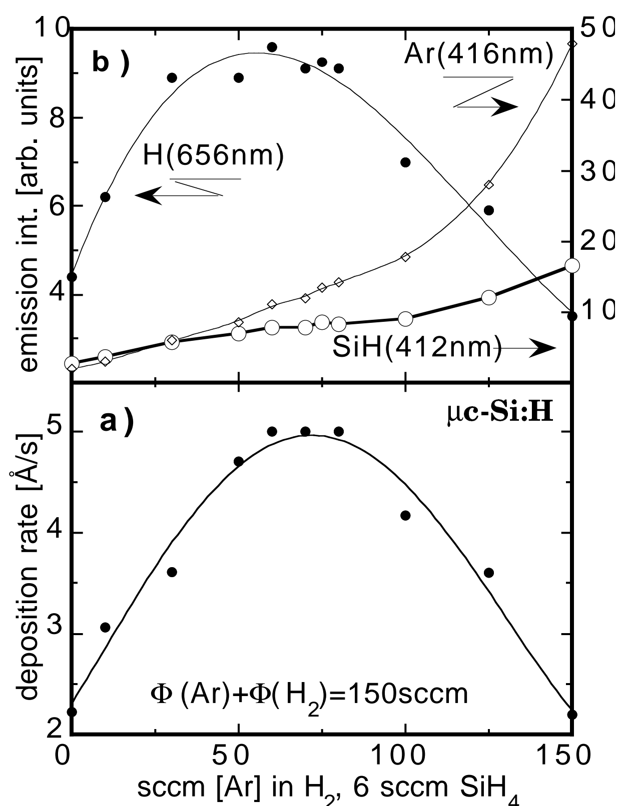


Fig. 4 M-series: a: deposition rate of µc-Si:H in function of the Ar/$H_2$ mixture at constant silane flow; b: emission lines from the plasma. Note that the Hα (656 nm) emission intensity correlates well with the deposition rate as observed in 4a.

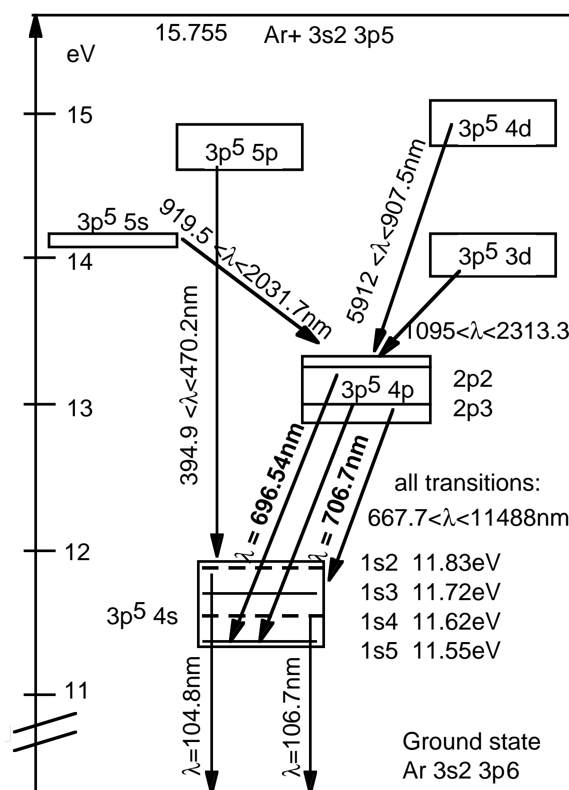


Fig. 5. Schematic energy levels of the argon atom, according to Ferreira et al [23]. The transients that are marked give are related to the rate of populating of the metastable state $1s_5$

As soon as argon partly replaces hydrogen in the diluting gas at constant silane concentration, the deposition rate of μc-Si:H increases. Note that all layers presented in the M series are microcrystalline.

Looking at plasma chemistry, the symmetrical shape of the plot in Fig 4a might be helpful for understanding the significant increase in deposition rate. As is well known from Hot-Wire experiments [22], the rate-limiting factor for μc-Si:H deposition is not related to the depletion of silane but rather to its dissociation.

Let us first consider the extreme cases at the boundaries of Fig. 4a phenomenologically: On one side (100% hydrogen dilution), a supporting contribution to the further radicalisation of $SiH_4$ due to the presence of argon is lacking; on the other side (100% argon dilution), a supporting contribution due to the presence of hydrogen is lacking. In both extreme cases, the lowest rate of about 2.2 Å/s is observed. In the intermediate range, both gases contribute equally to enhanced dissociation of silane. In order to explain this, we have to consider the different reaction channels with their respective reaction rates: The supporting contribution of argon in the silane plasma can be attributed to the creation of metastable states, as was already explained before in detail by several publications [18, 19, 23]. Hereby, the following fact should be mentioned: The creation of argon metastables (e.g. the Ar* ($^3P_2$) state ) from the argon ground state, is due to electron impact excitation. Note that electron impact does not necessarily directly lead to the creation of metastable states (called here Ar*), but first mostly to the population of states of higher argon levels (e.g. Ar $3p^5 4p$), see Fig. 5. This first step of excitation requires a threshold energy of 13.27 eV, i.e. it requires hot electrons. In a second step the emission of light at 696 and 706 nm (see in Figs. 3, 5) due to the rate of depopulation of the states $2p_2$ or $2p_3$ gives information on the rate of populating of the metastable state $1s_5$. On the other hand, collision of silane molecules with an argon atom in the metastable state can lead to the so-called molecular quenching reactions of metastables due to silane (2):

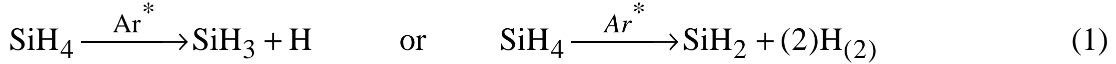

$$SiH_4 \xrightarrow{Ar^*} SiH_3 + H \quad \text{or} \quad SiH_4 \xrightarrow{Ar^*} SiH_2 + (2)H_{(2)} \qquad (1)$$

These reactions become the dominant loss mechanism for the occupation of metastable states **only** in strongly diluted silane plasmas (4% according to [18]), because comparatively more "hot" electrons are than available for the creation of metastables. If more silane is in the feedgas, more hot electrons of the energy distribution function are consumed for exciting silane via the different excitation channels instead of being available for the creation of metastables. We may assume, hence, that the dissociation of silane via metastable state quenching can indeed play a more important role in the deposition of μc-Si:H, as compared to the deposition of a-Si:H, because the conditions related to highly diluted silane are indeed prevalent in the case of μc-Si:H. For an explanation of the results given in Fig. 4a we propose the following model:

$$C(\text{total}) = \underbrace{C(SiH_4)}_{\text{const}} + \underbrace{C(H_2)}_{=0 \text{ for } 0\%\ H_2} + \underbrace{C(Ar)}_{=0 \text{ for } 0\%\ Ar} \qquad (2)$$

where C(total) is the concentration of all radicals that contribute to the formation of μc-Si:H; $C(SiH_4)$, $C(H_2)$ and C(Ar) are the contributions of radicals formed from $SiH_4$, $H_2$ and Ar, respectively. The reactions and their rate constants are given in the columns of Tab. 3.

Looking at Tab. 3, the respective reaction rates can be calculated from their rate constants and their concentration of prime components, using equations similar to the following equation (4). In equation (4) we will take, as an example, the Ar* quenching due to silane:

$$\frac{dSiH_4}{dt} = k_{Ar*}[SiH_4] \cdot [Ar*] \qquad (3)$$

| C ($SiH_4$) | C ($H_2$) | C(Ar) | |
|---|---|---|---|
| $SiH_4 \xrightarrow{e} SiH_3 + H$ k=1.59 x $10^{-10}$ $SiH_4 \xrightarrow{e} SiH_2 + (2)H_{(2)}$ k=1.87 x $10^{-11}$ | $H_2 \xrightarrow{e} 2\ H$ k=4.49 x $10^{-12}$ | $Ar \xrightarrow{e} Ar^*$ k=1.21 x $10^{-12}$ | electron impact |
| $SiH_4 \xrightarrow{H} SiH_3 + H_2$ k=2.68 x $10^{-11}$ | $SiH_4 \xrightarrow{H} SiH_3 + H_2$ k=2.68 x $10^{-11}$ | | hydrogen abstraction |
| | $H_2 \xrightarrow{Ar^*} 2\ H$ k=7 x $10^{-11}$ | $SiH_4 \xrightarrow{Ar^*} SiH_3 + H$ k=1.4 x $10^{-10}$ $SiH_4 \xrightarrow{Ar^*} SiH_2 + (2)H_{(2)}$ k =2.6 x $10^{-10}$ | molecular quenching |
| 3.8 % $SiH_4$ in total | 0-92.3% $H_2$ in total | 0-92.3% Ar in total | |

Tab. 3. Most important reaction channels for silane dissociation due to electron impact, hydrogen abstraction and molecular quenching. The rate constants are given in [$cm^3$/s]; the data are taken from Kushner [24] with references therein.

On the left side of Fig. 5a, the ensemble of all radical contributions given in the columns C($SiH_4$) and C($H_2$) of Tab. 3 lead to the poor rate of 2.2Å/s. On the right side of Fig. 4a, all equations of the columns C($SiH_4$) and C(Ar) lead to about the same low deposition rate. One might be led to assume, now, looking at Tab. 3 that a combination of all three columns at equal contributions of C($H_2$) and C(Ar) could perhaps explain the increase of the deposition rate as observed in Fig. 4a. However, a more detailed analysis is called for and will lead to a different conclusion. In our simple model only the most important reaction channels are taken into account; Furthermore, no steady-state concentrations can be determined due to the lack of data regarding the loss mechanisms. However, we know that the C(Ar) column in Tab. 3 should contribute, in the case of 100% Ar dilution much more than in the corresponding case of 100 % $H_2$, the C($H_2$) column; this results from the high production rate of metastables and its high rate constants for the molecular quenching channels. The only common reaction between argon and hydrogen that is characteristic for equal dilution with hydrogen and argon, is the quenching reaction of argon metastables via molecular hydrogen. However, both the rate constant and the concentration of the components of this reaction can be estimated to be much smaller than the contribution of C(Ar). Hence, we may indeed conclude that our simple plasma chemistry model given in Tab. 3 can in fact not explain the increase of the deposition rate of more than the factor of two as we observe in the M-series.

Hence, there must be an additional, much stronger contribution due to hydrogen that competes with the enhanced production of radicals as given by the column C(Ar). As a possible further explanation, we may assume that the chemisorbed hydrogen at the growing surface is etched away by atomic hydrogen and allows, by that, better sticking of radicals. This effect was postulated [25, 26] to be the rate-limiting mechanism for the deposition of amorphous and microcrystalline silicon. The rate limitation at 100% hydrogen dilution is due to the lack of radicals (left side of Fig. 5a); at 100% argon dilution, however, sufficient radicals are created but, according to this model, they all can not stick and are repelled into the plasma. Hence, at 100 % argon dilution, the deposition rate limiting factor is, as we now propose, due to sticking. Fig. 4b shows a good correlation between the emission intensity of the $H\alpha$ line at 656 nm and the deposition rate, whereas the intensities of all the other lines have the tendency to increase for

increasing argon dilution. We propose that for the M-series, the Hα line should be considered to be, indeed, a good monitor for the deposition rate.

Result on D-series.

Looking at the **D series** in Fig. 6a and Fig. 6b, the situation changes w.r.t. Fig. 4a and Fig. 4b: The increase in silane concentration in the feedgas from 3.2% silane to 7.4% in the mixture leads to an increase in deposition rate up to values as high as 9.4 Å/s the highest deposition rate we have observed in the present study. As found also for the M-series, all samples in the D-series are microcrystalline.

The evaluation of the spectral lines given in Fig. 6b show an increase of the intensity of the SiH* line at 412nm that correlates with the deposition rate. The line intensities of Ar and H, however, remain unchanged for lower concentrations of $SiH_4$ in the feedgas; for higher concentrations all intensities have a tendency to decrease. From Fig. 6 a,b one has to conclude for the D series that the emission intensity of the Hα line at 656 nm can here no more be used as a monitor of the deposition rate, whereas the SiH* line at 412 nm correlates better, in this specific case.

The **P-series** represented in Figs. 7a,b shows a surprising behaviour: The samples at 10W and 20W are amorphous silicon. At 30 W, μc-Si:H silicon is grown, at the maximum deposition rate within the P-series. Going to higher power, a pronounced reduction in deposition rate can be observed. All the emission lines in Fig. 7b increase with the power until a plateau is reached. Comparing Fig. 7a and 7b, no correlation between the deposition rate and any spectral line can be deduced.

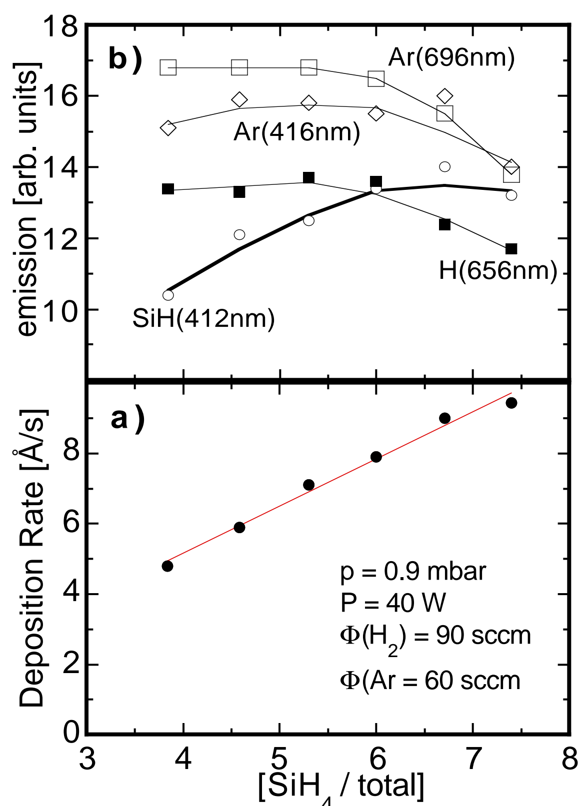


Fig. 6 a, b: D-series: Deposition rate of μc-Si:H in function of silane dilution and its comparison with the intensity of certain OES lines.

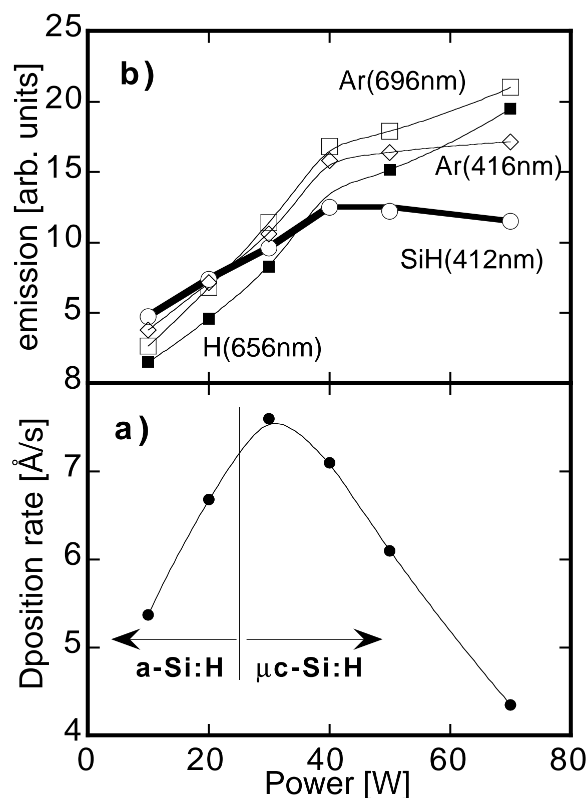


Fig. 7 a, b: P-series: Deposition rate of μc-Si:H in function of plasma power and its comparison with the intensity of OES lines.

From this behaviour of the P-series one can conclude, that the deposition rate of μc-Si:H can not be increased only by simply increasing the VHF power; for each set of $H_2$/Ar dilution an optimum set of pressure, $SiH_4$ flow and plasma power has to be individually determined.

Structural Properties

In the following, the structural consideration are mainly presented for the D-series; in fact this it is within this series that the highest deposition rate could be obtained in accordance with the main emphasis of this work.

X-Ray diffraction.

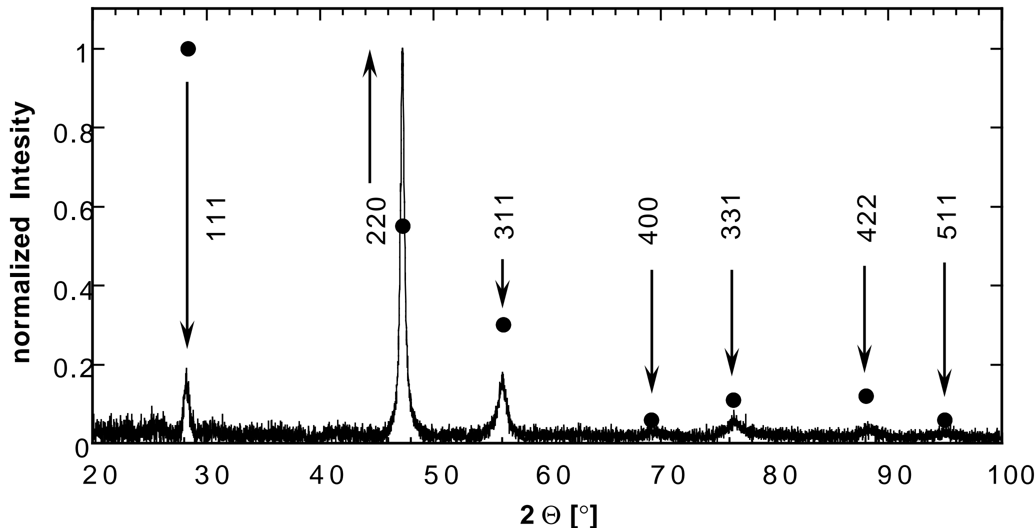


Fig. 8: Typical X-Ray diffraction pattern of a µc-Si:H thin film grown in an argon /hydrogen mixture. In contrast with powder samples, the 220 peak is very pronounced. The comparison with the round filled symbols (Si powder sample) is an indication of the strongly oriented growth of these µc-Si:H samples.

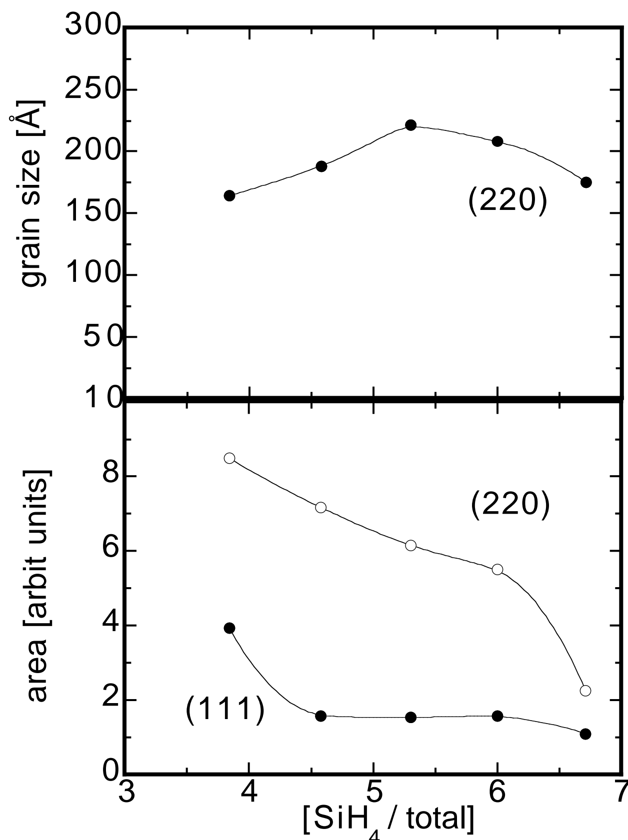


Fig. 9 Peak areas of the (111) and (220) X-Ray diffraction of the D-series; as well as apparent grain size of the D-series taken from the 220 signal and calculated by Scherrer's equation.

The X-Ray diffraction patterns of the samples of series M, D, P are all similar to the one shown in Fig. 8. We have strongly anisotropical columnar growth in the 220 direction. The specific pattern shown in Fig. 10 belongs exceptionally to the M series (75 sccm $H_2$; 75 sccm Ar; 6 sccm $SiH_4$).

From Fig. 8 we may conclude that the crystalline growth in our µc-Si:H samples is strongly oriented. We will now try to calculate the gain-size by applying Scherrer's formula, based on the (220) diffraction. Thereby, we will not determine the true grain-size, because our crystallites are not spherical, rather, we will find an apparent grain-size.

From SEM and TEM images the grains were found to be of columnar shape, see work of Meier et al. [9]. Still, a large apparent grain-size can be assumed to give, together with a strong anisotropy (as indicated by an anomalously large difference in the (111) and (220) X-ray diffraction value), means that there are probably no or only few grain-boundaries perpendicular to the direction of the photocurrent in a cell. Details of such a study are given elsewhere [27].

Infrared measurements.

The infrared measurements reveal two features: first, the Si-$H_x$ stretching mode does not show a pronounced shift from 2000 $cm^{-1}$ to 2100 $cm^{-1}$ as usually seen for the a-Si:H-µc-Si:H transition for the case of low concentrations of silane in an $Ar/H_2$ mixture (Fig. 10a). This is in agreement with results recently reported from Das et al. [19]; these authors diluted silane in pure argon.
Presumably, due to the presence of argon in the plasma, hydrogen is differently bonded in the resulting µc-Si:H layers. As reported by Kroll at al. [28] (using VHF-GD and only $H_2$-dilution). The phase transition from amorphous to microcrystalline silicon is usually related to a shift of the peak from 2000 to 2100 wavenumbers.
For µc-Si:H the 2100 $cm^{-1}$ peak is attributed to bonded hydrogen on crystallite surfaces.

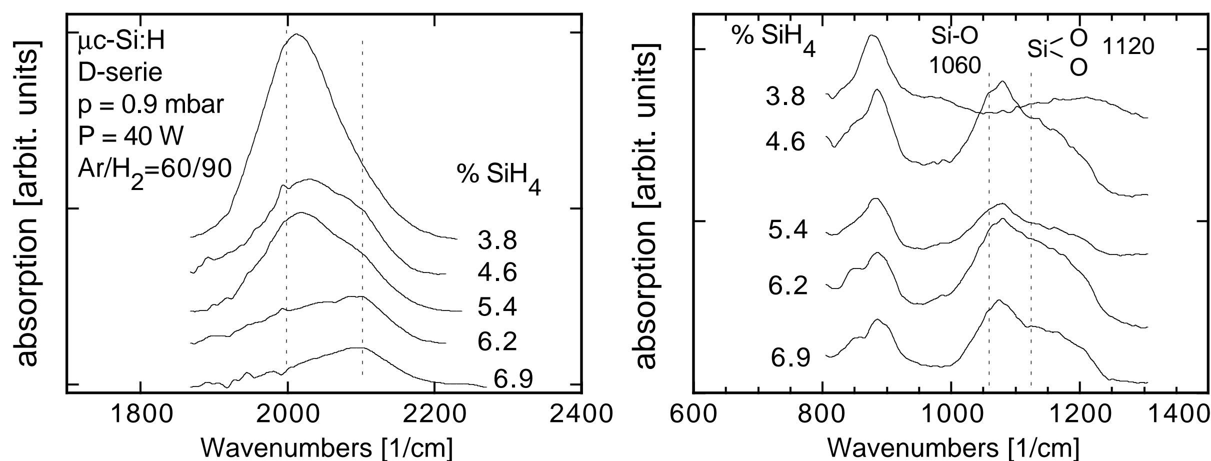


Fig. 10 a. Si-$H_x$ stretching mode of the samples of D-series. Note, usually the peak at 2100 1/cm is typical for microcrystalline silicon.

Fig. 10 b. In some of the samples of D-series, fingerprints for incorporated oxygen are found. The amount can not be correlated neither to the deposition conditions, nor to exposure at air.

Secondly, significant quantities of bonded oxygen in the layers are observed from the 1060 $cm^{-1}$ and 1120 $cm^{-1}$ modes (see Fig. 10b). The relative quantity of oxygen can not be correlated w.r.t. either the control parameters of the plasma (power, gas flow, pressure, dilution) nor with the post-oxidation after air-exposure. Note that in some cases, oxygen was observed to diffuse within two weeks into the layers [11]. This, however, does not seem to be the case for our samples.

As an explanation for the origin of oxygen in these layers, we postulate that the metastable states of the argon atoms play an important role in connection with water vapour in the feed gas. Enhanced oxygen incorporation was in fact previously already found by Kroll et al. [15] by SIMS measurements performed on a-Si:H layers that were deposited using argon-diluted silane. Using the gas-purifying technique, these authors could successfully suppress oxygen in the a-Si:H layers.

As all the experiment on individual layers we present here (series M, D, P) were undertaken without using the purifying technique, we may assume, that the following reaction gave rise to oxygen incorporation:

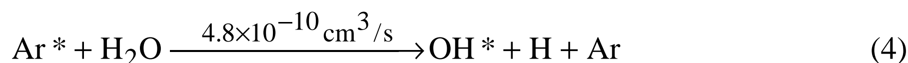

$$Ar^* + H_2O \xrightarrow{4.8\times10^{-10}\,cm^3/s} OH^* + H + Ar \qquad (4)$$

Velazco et al [29] found, that water vapour is an even more efficient "quencher" for Ar* metastables than silane. We deduce therefore, that in the case of Ar/$H_2$-dilution high deposition rates of μc-Si:H rate deposition becomes possible; however, water-vapour quenching of Ar* metastables has to be suppressed here, e.g. using a purifier in the gas lines.

Subbandgap absorption

Fig. 11 shows a comparison between the infrared absorption of our sofar best μc-Si:H samples according to previous work of Meier et al. [9] (called here "μc-Si:H Ref"), crystalline silicon, amorphous silicon, and our present high-rate deposited μc-Si:H, obtained using Ar/$H_2$ dilution.

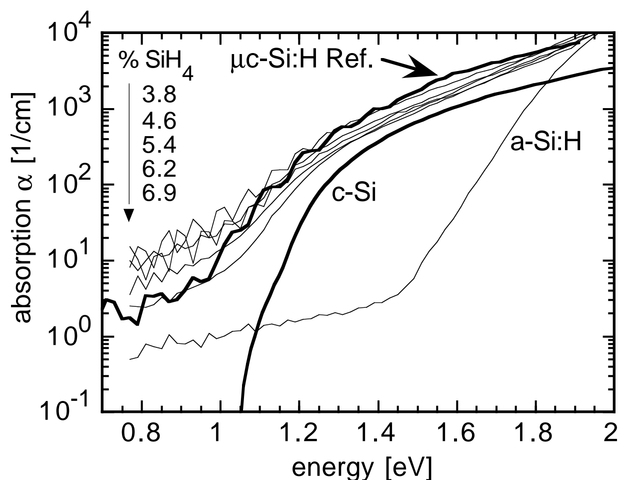


Fig. 11. Comparison of our sofar best μc-Si:H ("μc-Si:H Ref."), c-Si, a-Si:H and high-rate deposited μc-Si:H from the present series D.

It can be seen from Fig. 11 that the absorption around 1.2 eV for the new samples turns out to be lower than the previous values obtained with the previous sample indicated as "μc-Si:H Ref." This is an undesired effect for future solar cell applications, because the gain in deposition rate is partly offset by a loss in absorption around 1.2 eV; a fact which indeed requires thicker cells.

However, at the present state of the work, and looking at the strong oxygen incorporation of most of the samples in our present of the D-series, it should not be concluded in any way that high-rate deposited material has, as a general feature, a lower infrared absorption.

It was furthermore observed in this study that the material with the highest deposition rate (9.4 Å/s) showed the lowest subbandgap absorption within the present series; furthermore, all layers have an overall higher absorption than c-Si.

Results on solar cells.

A first attempt in fabricating an entirely μc-Si:H n-i-p solar cell with an i-layer deposited at 8.7 Å/s using Ar/$H_2$ diluted silane resulted in a cell efficiency of 3.15 %. The thickness of the i-layer was about 5.5 μm [27]. Here, a gas purifier was used while depositing this cell.

## 5. CONCLUSIONS

A silicon-based tandem solar cell called the "micromorph" solar cell containing a microcrystalline silicon bottom cell and an amorphous silicon top cell has obtained a stable efficiency of 10.7 %. Because of the relatively low absorption coefficient in the near infrared, a thick microcrystalline i-layer had to be applied: hence, this results in rather long deposition times result; thus this remains a major problem to overcome. Argon / hydrogen dilution of silane, as the method that was used here, in combination with the VHF-GD process, basically provides the possibility to achieve deposition rates up to 10 Å/s. Argon/hydrogen dilution experiments show, furthermore, that the columnar growth structure and the average grain-size of the crystallites can,

indeed, be controlled within a certain range. Thanks to the addition of argon as dilution gas, the parameter space that allows one to "tune" μc-Si:H w.r.t solar cell requirements is strongly expanded. Special care must thereby be taken in looking at all gases involved in the plasma: it was e.g. found that water vapour in the discharge leads to a pronounced incorporation of oxygen impurities into the growing film. It is concluded, therefore, that the use of a gas purifier becomes imperative for this particular method. The infrared absorption around 1.2 eV was lower in the present high-rate deposited microcrystalline silicon layers than in previous layers deposited by the VHF-GD in our group. This again, may be due to the enhanced oxygen incorporation that results from the use of argon as one of the dilution gas.
A first trial check with such high-rate material already result e.g. in a cell with 3.15 % efficiency. Thereby, an oxygen purifier was used, but the cell parameters were sofar not optimised.

ACKNOWLEDGEMENTS

This work was supported by the Swiss Federal Energy Department under Research Grant EF-REN (93)032

REFERENCES

1. J. Meier, R. Flückiger, H. Keppner, A. Shah, Appl. Phys. Lett., Vol. 65 (7), pp. 860-862, 1994.
2. P. Torres, J. Meier, M. Goetz, N. Beck, U. Kroll, H. Keppner, A. Shah, this conference.
3. S. Veprek and V. Marecek, Solid State Electronics Nr. 11, p. 683, 1968.
4. C. Wang and G. Lucowsky, Proc. 21st IEEE Photovoltaic Specialists Conference, Orlando 1990, Vol. 2, pp 1614-1618.
5. M. Faraj, S. Gokhale, S. M. Choudhari, and M. G. Takwale, Appl. Phys. Lett. 60, p. 3289, 1992.
6. R. Flückiger, J. Meier, H. Keppner, U. Kroll, A. Shah, O. Greim, M. Morris, J. Pohl, P. Hapke, R. Carius, Proceedings of the 11th EC Photovoltaic Solar Energy Conference, Montreux, 1992, p. 617.
7. J. Meier, S. Dubail, D. Fischer, J. A. Anna Selvan, N. Pellaton Vaucher, R. Platz, C. Hof, R. Flückiger, U. Kroll, N. Wyrsch, P. Torres, H. Keppner, A. Shah, K.-D. Ufert, Proceedings of the 13th EC Photovoltaic Solar Energy Conference, Nice, 1995, p. 1445.
8. J. Meier, S. Dubail, R. Flückiger, D. Fischer, H. Keppner, A. Shah, Proceedings of the 1st World Conference on Photovoltaic Energy Conversion, Hawaii, 1994, Vol. 1, pp. 409-412.
9. J. Meier, P. Torres, R. Platz, S. Dubail, U. Kroll, J.A. Anna Selvan, N. Pellaton-Vaucher, Ch. Hof, D. Fischer, H. Keppner, A. Shah, K.-D. Ufert, P. Giannoulès, J. Koehler, to be published in the Proc. MRS 1996 Spring Meeting San Francisco.
10. D. Fischer, S. Dubail, J.A. Anna Selvan, N. Pellaton-Vaucher, R. Platz, Ch. Hof, U. Kroll, J. Meier, P.Torres, H. Keppner, N. Wyrsch, M. Goetz, A. Shah, K.-D. Ufert, Proc. 25th IEEE Photovoltaic Specialists Conference , Washington , 1996, Vol. 2 pp. 1053-1056.
11. S. Veprek, Z. Iqbal, R. O. Kühne, P. Capezzuto, F-A Sarott and J. K. Gimzewski, J. Phys. C: Solid State Physics, 16, pp. 6241-6262, 1983.
12. U. Kroll, J. Meier, H. Keppner, and A. Shah, J. Vac. Sci. Technol. A 13(6) p. 2742, 1995.
13. F. Finger, P.Hapke, M. Lysberg, R. Carius, H. Wagner, Appl. Phys. Lett. 65(20), p. 247,1994.
14. A. Matsuda, S. Mashima, K. Hasezaki, A. Suzuki, S. Yamasaki and P.J. McElhenny, Appl. Phys. Lett., 58, p. 2494, 1991.

15. U. Kroll, PhD thesis University of Neuchâtel, Hartung & Gorre Verlag, Konstanz, ISBN 3-89191-905-0, 1995.
16. J. Hautala, Z. Saleh, J.F.M. Westendorp, H. Meiling, S. Sherman, and S. Wagner, to be published in the Proceedings of the MRS Spring Meeting, San Francisco, Vol. 420, 1996.
17. N. Imajyo, J. of Non-Cryst. Solids, 198-200, pp. 935-939, 1995.
18. L. Sansonnens, A.A. Howling, Ch. Hollenstein, J-L. Dorier, and U. Kroll, J. Phys. D: Appl. Phys. 27, pp 1406-1411, 1994.
19. U. K. Das and P. Chaudhuri, S.T. Kshirsagar, J. Appl. Phys. 80(9) pp. 5389-5397, 1996.
20. J. Perrin, J. Schmitt, Chem. Phys. 67, p. 167, 1982.
21. T. Hamasaki, H. Kurata, M. Hirose, and Y. Osaka, Appl. Phys. Lett. 37, p. 1084, 1980.
22. A. R. Middya, J. Guillet, J. Perrin, A. Lloret, and J. E. Bourrée, Proceedings of the 13th EC PV Conference, Nice, 1995, p. 1704.
23. C. M. Ferreira and J. Loureiro, J. Appl. Phys. 57(1), p. 82, 1985.
24. M. J. Kushner, J. Appl. Phys. 63(8), p. 2532, 1988.
25. S. Veprek, F. -A. Sarrott and S. Rambert, E. Taglauer, J. Vac. Sci. Technol. A 7(4) p. 2614, 1989.
26. M. Heintze and R. Zedlitz, Progress in Photovoltaics: Research and applications, 1, p. 213, 1993.
27. H. Keppner, U. Kroll, P. Torres, J. Meier, R. Platz, D. Fischer, N. Beck, S. Dubail, J.A. Anna Selvan, N. Pellaton Vaucher, M. Goerlitzer, Y. Ziegler, R. Tscharner, Ch. Hof, M. Goetz, P. Pernet, N. Wyrsch, J. Vuille, J. Cuperus, and A. Shah, to be published at the NREL/SNL Photovoltaics Program review Meeting, Lakewood Co, 1996.
28 U. Kroll, J. Meier, A. Shah, S. Mikahaiov, J. Weber, J. Appl. Phys. 80, p. 4971, 1996.
29. J. E. Velazco, J. H. Kolts, D. W. Setser, J. Chem. Phys., 69(10), p. 4357, 1978.